

Inertia triggers nonergodicity of fractional Brownian motion

Andrey G. Cherstvy ^{1,2,*}, Wei Wang ^{3,†}, Ralf Metzler ^{2,‡} and Igor M. Sokolov ^{1,4,§}

¹*Institut für Physik, Humboldt-Universität zu Berlin, Newtonstraße 15, 12489 Berlin, Germany*

²*Institute for Physics & Astronomy, University of Potsdam, Karl-Liebknecht-Straße 24/25, 14476 Potsdam-Golm, Germany*

³*Max Planck Institute for the Physics of Complex Systems, Nöthnitzer Straße 38, 01187 Dresden, Germany*

⁴*IRIS Adlershof, Zum Großen Windkanal 6, 12489 Berlin, Germany*



(Received 17 June 2021; accepted 29 July 2021; published 13 August 2021)

How related are the ergodic properties of the over- and underdamped Langevin equations driven by fractional Gaussian noise? We here find that for massive particles performing fractional Brownian motion (FBM) inertial effects not only destroy the stylized fact of the equivalence of the ensemble-averaged mean-squared displacement (MSD) to the time-averaged MSD (TAMSD) of overdamped or massless FBM, but also dramatically alter the values of the ergodicity-breaking parameter (EB). Our theoretical results for the behavior of EB for underdamped or massive FBM for varying particle mass m , Hurst exponent H , and trace length T are in excellent agreement with the findings of stochastic computer simulations. The current results can be of interest for the experimental community employing various single-particle-tracking techniques and aiming at assessing the degree of nonergodicity for the recorded time series (studying, e.g., the behavior of EB versus lag time). To infer FBM as a realizable model of anomalous diffusion for a set single-particle-tracking data when massive particles are being tracked, the EBs from the data should be compared to EBs of massive (rather than massless) FBM.

DOI: [10.1103/PhysRevE.104.024115](https://doi.org/10.1103/PhysRevE.104.024115)

I. INTRODUCTION

Fractional Brownian motion (fractional BM or FBM)—introduced by Kolmogorov [1] and further developed by Mandelbrot and van Ness [2]—is one of the paradigmatic stochastic anomalous-diffusion processes [3–6] employed to describe or rationalize numerous experimental observations of non-Brownian or nonlinear diffusion taking place on various length- and timescales, from the nanoworld to the interstellar space (the list of relevant studies is too long to overview it in this short paper). In its classical formulation, the dynamics of a single FBM particle is described by the overdamped Langevin equation (the high-friction scenario) [7–13]

$$dx(t)/dt = \eta_H(t) \quad (1)$$

driven by fractional Gaussian noise $\eta_H(t)$ with zero mean and power-law long-ranged correlations, with (for $t \neq t'$)

$$\langle \eta_H(t)\eta_H(t') \rangle \simeq K_{2H}2H(2H-1)|t-t'|^{2(H-1)}. \quad (2)$$

For “athermal” FBM dynamics—with no (generalized) fluctuation-dissipation relation being fulfilled, in contrast to BM—the mean-squared displacement (MSD)

$$\langle x^2(t) \rangle = \int x^2 P(x, t) dx = 2K_{2H}t^{2H} \quad (3)$$

follows from the probability-density function, which for the Dirac-delta-like initial condition, $P(t=0) = \delta(x-x_0)$, is given by the Gaussian

$$P(x, t) = \exp\left[-\frac{x^2}{4K_{2H}t^{2H}}\right] / \sqrt{4\pi K_{2H}t^{2H}}. \quad (4)$$

Here K_{2H} is the generalized diffusion coefficient (with the physical units $[K_{2H}] = \text{m}^2/\text{sec}^{2H}$) and H is the Hurst exponent [3,6]. The increments of FBM are positively (negatively) correlated for superdiffusive (subdiffusive) Hurst exponents, for $1 > H > 1/2$ and $0 < H < 1/2$, respectively. Standard BM is FBM at $H = 1/2$.

From a time series $x(t)$ of a stochastic process, the time-averaged MSD (TAMSD) is defined as the sliding average of squared increments along the trajectory of length T as

$$\overline{\delta^2(\Delta)} = \frac{1}{T-\Delta} \int_0^{T-\Delta} [x(t+\Delta) - x(t)]^2 dt, \quad (5)$$

where Δ is the lag time. Averaging over N realizations of a fluctuating variable $\delta^2(\Delta)$ constructed via (5) from $x(t)$, the mean TAMSD at a given Δ value is

$$\langle \overline{\delta^2(\Delta)} \rangle = \frac{1}{N} \sum_{i=1}^N \overline{\delta_i^2(\Delta)}. \quad (6)$$

Hereafter, the angular brackets denote ensemble averaging, while time averaging is shown by the overline. The standard concept of ergodicity [3,6,14–20] (see Refs. [21–24] for some alternative approaches) implies the equivalence of the MSD to the [mean] TAMSD for long trajectories and short lag times,

*a.cherstvy@gmail.com

†weiwangnuaa@gmail.com

‡rmetzler@uni-potsdam.de

§igor.sokolov@physik.hu-berlin.de

at $\Delta/T \ll 1$. FBM is ergodic [7–9,13], with

$$\overline{\langle \delta^2(\Delta) \rangle} = 2K_{2H} \Delta^{2H} = \langle x^2(\Delta) \rangle. \quad (7)$$

The degree of nonergodicity—or of innate irreproducibility of the TAMSD realizations—is quantified by the ergodicity-breaking parameter [6,7,25–28],

$$\text{EB}(\Delta) = \langle \overline{\langle \delta^2(\Delta) \rangle} \rangle / \overline{\langle \delta^2(\Delta) \rangle}^2 - 1 = \langle \xi^2(\Delta) \rangle - 1, \quad (8)$$

that is the ratio of the variance to the squared mean of $\overline{\langle \delta^2(\Delta) \rangle}$. The dispersion and distribution of the TAMSDs (5) around their mean (6) is embodied in the distribution $\phi(\xi)$, where $\xi(\Delta) = \overline{\langle \delta^2(\Delta) \rangle} / \langle \delta^2(\Delta) \rangle$.

In the continuous-time framework, EB of FBM for the Hurst exponent $0 < H < 3/4$ deviates only slightly from EB for BM given by,

$$\text{EB}(\Delta) \approx 4\Delta/(3T), \quad (9)$$

growing at $\Delta/T \ll 1$ as [7] [see Eq. (18) below] $\text{EB}(\Delta) \approx C_1(H) \times (\Delta/T)^1$. For $1 > H > 3/4$ the behavior of $\text{EB}(\Delta)$ of FBM is more subtle: the EB values also depend explicitly on the lag time [rather than only on the (Δ/T) ratio], with EBs being generally significantly larger. In this range of H exponents FBM features a slower approach to ergodicity: we refer to [7,12,29–32] for the continuous-time and to Refs. [13,33] for the discrete-time calculations of EB for FBM.

Our key objective here is to quantify (non-)ergodicity of FBM in terms of EB for diffusion of massive—rather than massless—particles. We focus on the experimentally relevant setup of a constant trace length T and varying particle mass m , as often utilized in EB calculations [e.g., for size- or mass-polydisperse tracers in single-particle-tracking (SPT) and optical-tweezers-based [34–38] experiments]. We use underdamped or massive and overdamped or massless interchangeably for the respective scenarios of FBM diffusion. FBM particles with $m \neq 0$ require an underdamped description yielding an additional timescale; see below.

The paper is organized as follows. Starting with the description of the simulation scheme in Sec. II A, in Sec. II B the results for the MSD and mean TAMSD of underdamped FBM are presented, from both computer simulations and theory. In Sec. II C the main results for the EB parameter of massive FBM are presented and contrasted to those for massless FBM. We conclude in Sec. III and mention some applications. In Appendix A certain technical details and derivations are given, while some auxiliary figures are presented in Appendix B.

II. MAIN RESULTS

A. Diffusion model and simulation scheme

We simulate the diffusion for a single tracer of mass m driven by external fractional Gaussian noise $\eta_H(t)$ using the underdamped Langevin equation,

$$m d^2 x(t)/dt^2 + \gamma dx(t)/dt = \gamma \eta_H(t), \quad (10)$$

used recently also in Refs. [39–42]. Here we consider the instantaneous Stokes damping, $-\gamma dx(t)/dt$, with a constant coefficient γ (not a dynamical Basset force; see, e.g., the discussion in Ref. [38]). We set $\gamma = 1$ below, so that the

characteristic momentum-relaxation or Smoluchowski’s time,

$$\tau_0 = m/\gamma, \quad (11)$$

is controlled in simulations (for simplicity) solely by the particle mass m . We study the potential-free case; the general problem of (non-)ergodicity of massive-FBM in the presence of a space-dependent potential is complicated and requires a special investigation.

To simulate (10) we introduce the velocity $v(t) = dx(t)/dt$ and discretize the resulting Eq. (A3) with the time step dt

$$x_{n+1} - x_n = v_n dt, \quad v_{n+1} - v_n = -\tau_0^{-1} v_n dt + \tau_0^{-1} (\Delta B_H)_n, \quad (12)$$

with $1 < n < (\bar{N} - 1)$, where

$$\bar{N} = T/dt \quad (13)$$

is the number of elementary steps in the trajectory. This system of forward recurrent equations is solved with the initial position x_0 and velocity v_0 of the particle. Both $v_0 = 0$ and v_0 being distributed according to the stationary-state distribution are considered. The increment of standard FBM $(\Delta B_H)_n$ is generated using the Wood-Chan method (faster than the Hosking approach) based on the fast Fourier transform [43].

B. MSD and TAMSD

In Fig. 1 we present the results of simulations for the MSD and TAMSD of massive-FBM particles starting their motion with $v_0 = 0$, for two values of the Hurst exponent H (for sub- and superdiffusive dynamics). We find that the long-time dynamics of massive FBM is expectedly the same as for massless FBM, with the MSD (3) being equal to the TAMSD (7). At short lag times the mean TAMSD of massive FBM start ballistically,

$$\overline{\langle \delta^2(\Delta) \rangle} \propto \Delta^2, \quad (14)$$

while its MSD grows superballistically,

$$\langle x^2(t) \rangle \propto t^{2H+2}. \quad (15)$$

The exact prefactors in these relations are derived in Appendices A 1 and A 2; see Eqs. (A29), (A31), and (A20), respectively. In terms of the MSD-to-TAMSD equivalence, underdamped FBM ceases to stay ergodic: both scalings and magnitudes of $\langle x^2(\Delta) \rangle$ and $\overline{\langle \delta^2(\Delta) \rangle}$ are disparate, see Fig. 1. Massive FBM also features larger EB values, see Sec. II C.

The long-time evolution of the MSD and TAMSD for massive FBM is identical, given by that of massless FBM in (3) and (7), namely,

$$\langle x^2(\Delta) \rangle = \overline{\langle \delta^2(\Delta) \rangle} = 2K_{2H} \Delta^{2H}. \quad (16)$$

The temporal extent of the short-time regimes given by (14) and (15) grows with the particle mass [similarly to that for massive BM or the Ornstein-Uhlenbeck (OU) process [44]] and depends on the Hurst exponent. These two parameters determine the “agility” of the underlying dynamics; compare Figs. 1 and 5 (see Appendix B for Figs. 5–11) for the 10-times heavier particles. Expressions (A23) and (A35) give the crossover times to the long-time behavior (16) of the MSD and mean TAMSD.

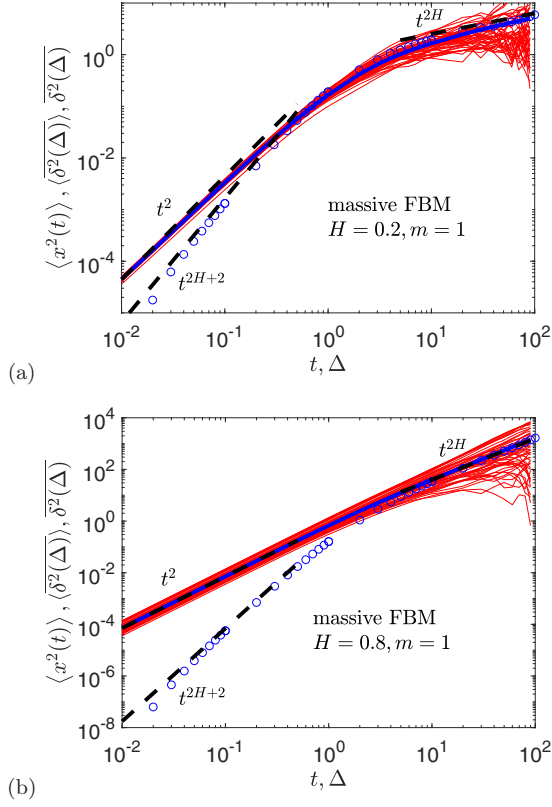


FIG. 1. Magnitude of the MSD $\langle x^2(t) \rangle$ (blue circles), the spread of individual TAMSDs $\delta^2(\Delta)$ (thin red curves), and the mean TAMSD $\overline{\delta^2(\Delta)}$ (thick blue curve) for massive FBM, shown for two values of the Hurst exponent (see the legends). The long-time MSD and mean TAMSD asymptotes given by expressions (3) and (7), respectively, are the dashed lines. The short-time asymptotes (15) and (14) for the MSD and mean TAMSD are the dashed lines. Parameters: the particle mass is $m = 1$, the time step of simulations is $dt = 10^{-2}$, the trajectory length is $T = 10^2$ (or 10^4 time steps), the number of independent trajectories used for ensemble averaging is $N = 10^3$, the initial conditions are $x_0 = 0$ (for this and all other plots) and $v_0 = 0$, and the generalized diffusivity is set at $K_{2H} = 1/2$.

We emphasize that initial velocities of the particles—instead of being zero as in Fig. 1—can be sampled from the stationary distribution (A12), with $\langle v^2 \rangle_{st}$ given by (A11). Then the MSD and mean TAMSD are *equal* and both acquire a transient short-time ballistic growth,

$$\langle x^2(\Delta) \rangle = \overline{\delta^2(\Delta)} \propto \Delta^2, \quad (17)$$

with a crossover time to the long-time behavior given by expression (A24). For stationary-state-distributed initial velocities, the process of massive FBM stays “ergodic” at short times in the sense of the MSD-to-TAMSD equivalence, whereas the long-time growth of the two averages is the same as for massless FBM given by expression (16) see Fig. 6 as well as Appendices A1 and A2. In analogy to superballistic tracer dispersion $\propto t^{2H+2}$ in Eq. (15) and the ballistic law (17) for massive FBM, for massive BM with constant or zero and stationary-state-distributed initial velocities of the particles the short-time MSD grows as $\propto t^3$ and $\propto t^2$, respectively (see the detailed discussion and the experimental confirmation of this in the seminal work [37]).

We stress, however, that despite (17) is true for the averages, the irreproducibility of individual TAMSDs increases for larger Hurst exponents, as quantified in Fig. 6(b). This increase has dramatic implications for the EB values characterizing the dispersion of $\delta^2(\Delta)$ around $\overline{\delta^2(\Delta)}$, see Sec. II C.

C. EB

1. Spread of $\overline{\delta^2(\Delta)}$

From Fig. 1 it becomes apparent that for superdiffusive underdamped FBM the individual TAMSDs become less reproducible. This fact gets reflected in larger values of the EB parameter, as compared to those for standard FBM [7,13], see the results of simulations in Fig. 7 for $EB(\Delta)$ for FBM with $H = 0.8$ and 0.2 (both for the under- and overdamped cases). The increase of EB for massive FBM is observed in the entire range of lag times, but at the shortest lag time $\Delta = \Delta_1 = dt$ it is particularly dramatic. This is associated with a larger degree of nonergodicity (in terms of EB [6]). This fact is relevant for SPT experiments as—in virtue of the best time-averaging statistics at short lag time—the time series are often used to compare the assessed $EB(\Delta_1)$ values to EBs of known models of diffusion [6,45–47]. We stress that for the massive particles driven by η_H —with the initial conditions $x_0 = 0$ and $v_0 = 0$ —the EB values are dramatically larger than those for overdamped FBM [7]. The deviations of massive versus massless FBM results for EB are (expectedly) the largest for lag times where the respective MSD and TAMSD deviate, compare the respective Δ -regions in Figs. 1 and 7. The number of independent *in silico*-generated trajectories used for ensemble averaging in Fig. 1 and all later plots is at least $N = 10^3$.

2. EB of massless FBM

In Fig. 7 we show for comparison the theoretical predictions for EB of massless FBM in the framework of *continuous* time given by [7,12,13]

$$EB(\Delta) \approx \begin{cases} C_1(H) \times (\Delta/T)^1, & 0 < H < 3/4 \\ C_2(H) \times (\Delta/T)^{4(1-H)}, & 1 > H > 3/4 \end{cases} \quad (18)$$

with the coefficients

$$C_1(H) = \int_0^\infty [(1+t')^{2H} + |1-t'|^{2H} - 2(t')^{2H}]^2 dt' \quad (19)$$

[see Fig. 8 of Ref. [13] for $C_1(H)$ values for some H] and

$$C_2(H) = [2H(2H-1)]^2 \left(\frac{1}{4H-3} - \frac{1}{4H-2} \right). \quad (20)$$

Here (Δ/T) is the only possible dimensionless time.

We also use the results for EB of massless FBM in the *discrete*-time approach [13,31], predicting that at the first step (for $H < 1/2$)

$$EB(\Delta_1, \bar{N}) \approx \frac{2}{\bar{N}-1} + \frac{(\bar{N}-2)(2^{2H}-2)^2}{(\bar{N}-1)^2}. \quad (21)$$

Here \bar{N} is given by Eq. (13). For $H > 1/2$ the result for $EB(\Delta_1, \bar{N})$ is more complicated, given by Eq. (C4) of

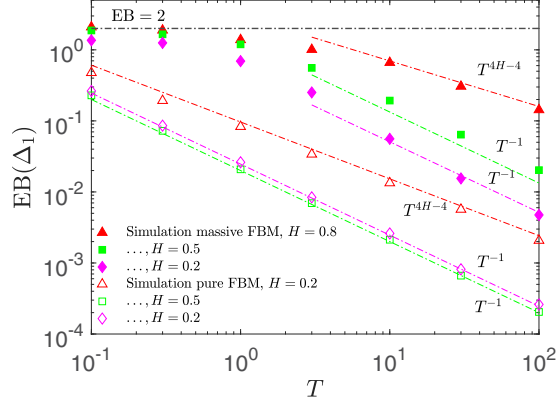


FIG. 2. EB of massive FBM versus trajectory length T for several values of the H exponent (the filled symbols), with the scaling relations (23) and (A53) shown as the dashed lines [no data fitting here, the exact prefactors used]. The results of EB simulations of massless FBM for the same H are the empty symbols; they are shown together with the modified Deng-Barkai [7] EB asymptote (18) and the discrete-time EB expression (21), see Ref. [13]. The initial velocities are $v_0 = 0$. Parameters: $m = 1$, $dt = 10^{-2}$.

Ref. [13]. The terminal value (see Ref. [13] for details)

$$\text{EB}(\Delta = T) = 2 \quad (22)$$

is also referred to in Fig. 7 and in other EB plots.

In Fig. 8 the variation of $\text{EB}(\Delta)$ of massive FBM—computed at the shortest lag time $\Delta = \Delta_1$ —with the Hurst exponent H is summarized. For underdamped FBM the behavior of $\text{EB}(\Delta_1)$ is very different from the discrete-time prediction (21) (see our recent study [13] for detailed derivations and description). Instead, we find that, starting from very small H , the values $\text{EB}(\Delta_1)$ grow quickly with H , rather than stay nearly constant in the range $0.6 \gtrsim H > 0$ as EB expression (21) would predict. At $\Delta \rightarrow T$ the value of $\text{EB}(\Delta)$ approaches (22).

3. EB of massive FBM

For a fixed m , for longer times series massive FBMs turn progressively “less heterogeneous” and deviations from ergodicity decrease. Specifically, $\text{EB}(\Delta_1, T)$ values obtained from simulations are found to decrease with the trajectory length T according to the empirical scaling

$$\text{EB}(\Delta_1, T) \sim \begin{cases} (\Delta_1/T)^1, & 0 < H < 3/4 \\ (\Delta_1/T)^{4(1-H)}, & 1 > H > 3/4 \end{cases} \quad (23)$$

as illustrated in Fig. 2. The approach to ergodicity for longer trajectories of massive-FBM particles is, thus, the same as that for standard FBM [7] in expression (18), with the anomalously slow EB decrease with T and slower approach to ergodicity for $1 > H > 3/4$. As follows from Fig. 2, for a fixed mass m , a slower decay of the EB parameter for massive FBM for increasing H requires longer trajectories for scaling (23) to be applicable. For comparison, the empty symbols in Fig. 2 are the results of simulations for the decay of $\text{EB}(\Delta_1, T)$ with T for massless FBM following Eq. (18).

Our main results, presented in Fig. 3, show that for vanishing mass m the EB values for massive FBM approach those

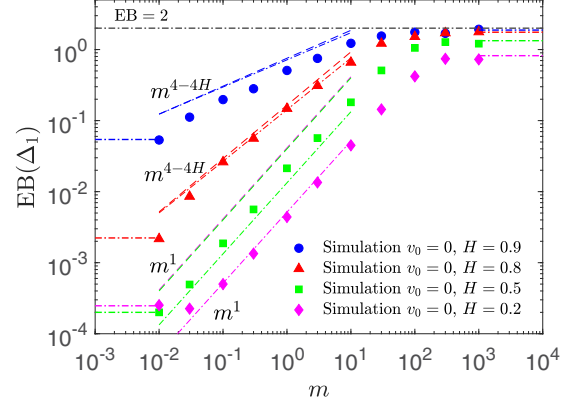


FIG. 3. EB parameter of underdamped FBM plotted versus the particle mass m for several H values. At intermediate m -values we show the scaling relations of Eqs. (24) and (A51) as the dashed colored lines and the EB expression (A53) with the exact prefactors (no data fitting) as the dot-dashed colored asymptotes. The terminal EB value (22) is also shown. The colored dot-dashed lines on the left and on the right side of the plot, respectively, indicate the discreteness-induced plateaus of EB for massless FBM in the discrete-time formulation given by (21) and the EB plateaus in the large-mass limit given by (A42). The initial velocities are $v_0 = 0$. Parameters: $T = 10^2$, $dt = 10^{-2}$.

of massless FBM, Eq. (21) in the discrete-time approach, as expected. For extremely massive particles, the EB parameter reaches its maximal values, saturating at H -dependent plateaus [see Eq. (A42) and the derivations in Appendix A3 and also Fig. 9]. These large EB values corroborate with the most pronounced spread of $\delta^2(\Delta)$ and, therefore, broader distributions $\phi(\xi(\Delta_1))$ for diffusion of heavier FBM particles (as detailed in Fig. 5, which is to be compared to Fig. 1).

For the particles of intermediate masses, we empirically find scaling relations

$$\text{EB}(\Delta_1, m) \sim \begin{cases} m^1, & 0 < H < 3/4 \\ m^{4(1-H)}, & 1 > H > 3/4 \end{cases} \quad (24)$$

which are in excellent agreement with the *in silico* results for all H values, see Fig. 3. In Appendix A3 we present the derivations of the EB plateaus for large-mass or short-trace conditions given by (A42) and the variation of EB for long trajectories given by expression (A51), both in excellent agreement with the results of simulations and identical to the empirical laws (23) and (24).

We stress that—although for stationary-state distribution of initial velocities (A12) of massive-FBM particles the TAMSD scaling gets affected and the short-time MSD-versus-TAMSD equivalence gets restored, as shown in Fig. 6—using the stationary-state distribution for v_0 does not change the scaling relations for the ergodicity-breaking parameter $\text{EB}(\Delta_1, m)$ versus particle mass m given by relations (24). These scaling relations are the same for the case $v_0 = 0$ and for $p_{\text{st}}(v_0)$ -distributed initial velocities, see the derivations of (A51) and (A53). Solely the EB-plateau values at $m \rightarrow \infty$ are different in these two scenarios, as evident from comparing Fig. 3 obtained for $v_0 = 0$ and Fig. 10 where the stationary distribution $p_{\text{st}}(v_0)$ given by (A12) was used.

III. DISCUSSION AND CONCLUSIONS

We examined the diffusion process driven by fractional Gaussian noise η_H in the presence of inertia, both analytically and via stochastic computer simulations. We found that the short-time transient mass-dependent growth of the MSD is superballistic with $\langle x^2(t) \rangle \propto t^{2H+2}$, while the mean TAMSD grows at short-lag-time ballistically, $\overline{\delta^2(\Delta)} \propto \Delta^2$. In this range of times—quantified in Appendices A 1 and A 2—a pronounced inertia-induced MSD-to-TAMSD nonequivalence was found. Systematically varying the Hurst exponent H and particle mass m we demonstrated that the evolution of the EB parameter at short lag times follows the scaling relations with trajectory length T and tracer mass m . In particular, EB for massive FBM grows with m at a fixed T , reaching much larger values than EBs of massless FBM. The scaling relations (23) and (24)—derived in Appendix A 3 as (A51) and (A53)—are closely supported by the results of simulations and embody the main findings of this study.

We emphasize that the effects of inertia, inevitable in the short-time behavior of real-world tracers in SPT experiments, should be carefully accounted for if a quantitative comparison of the computed EB values versus those for FBM (or other diffusion models) is to be performed. For short lag times—where the EB-averaging statistics is most accurate and, thus, often used in the SPT-data analysis—the values of EB were found to be most affected by these inertia effects. The emerging “ballistic” in the TAMSD and the altered scaling of the MSD in this short- Δ region was shown to trigger the MSD-to-TAMSD nonequivalence and weak ergodicity breaking for the η_H -driven dynamics of massive particles.

From the experimental perspective, the m - and H -dependent timescales—when the above-mentioned ballistic effects can play a role in the massive-FBM dynamics [see Eqs. (A23) and (A35)]—should be understood for a given tracer mass m , trajectory length T , lag time Δ , and properties of the diffusion medium (embodied by γ). This will clarify whether the short- or long-time asymptotic behaviors of the TAMSD and EB are valid for a given set of data and system parameters. The computed EB values—if aimed at a quantitative comparison with known models of massless-particle diffusion—should be properly *adjusted* to account for a finite particle mass, m . This is exemplified above for massive FBM.

From the theoretical perspective, the velocity-relaxation time $\tau_0 = m/\gamma$ in (11) naturally rescales the timescale T to be taken for a physically correct comparison of EB values for FBM computed for the particles of varying mass. As we have shown, the inertial effects make FBM appear nonergodic when, e.g., the trajectory length T is fixed while mass m is varied. A correct rescaling of the trace length T with a typical relaxation time τ_0 would be

$$T \rightarrow T_{m,\gamma} \equiv T/\tau_0, \quad (25)$$

so that heavier particles diffuse for the same *relative* time, $T_{m,\gamma}$. The relaxation time τ_0 is, therefore, an important physical timescale, as compared to a “scale-free” massless FBM. The mass-dependent T -rescaling (25) renders the respective $\text{EB}(\Delta = \Delta_1)$ values *universal and constant* for a fixed $T_{m,\gamma}$,

$$\text{EB}(\Delta_1, T, m, \gamma) \rightarrow \text{EB}(\Delta_1, T/[m/\gamma]). \quad (26)$$

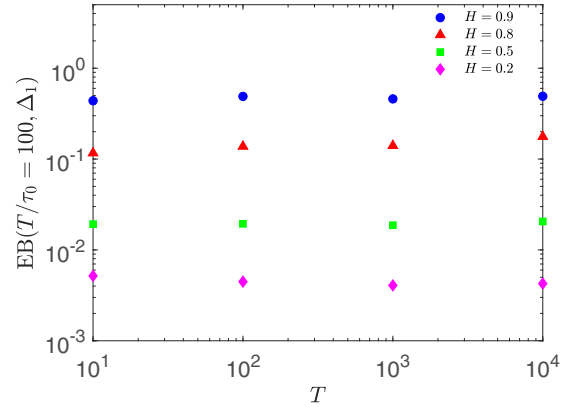


FIG. 4. Nearly constant EB of massive FBM at $\Delta_1 = 10^{-2}$ for *simultaneously* varying particle mass m and trajectory length T such that the *rescaled* trace length $T_{m,\gamma}$ in (25) stays constant, namely $T/\tau_0 = 10^2$. The initial velocities are $v_0 = 0$.

We have indeed confirmed this invariance of the rescaled EB parameters via simulating massive FBM for a constant $T_{m,\gamma}$ but for a set of different T and m values (see Fig. 4) for both sub- and superdiffusive H exponents. Note that a plateau-like behavior of EB at small Δ (especially for $H = 0.8$), as shown in Fig. 7, enables us to consider in Fig. 4 for rescaling (26) the EB values at the same Δ_1 for different T . The rescaling (25) is also supported by theoretical arguments in Appendix A 3: namely, EB in (A51) varies with the rescaled (τ_0/T) -variable only. We stress that a similar time-rescaling “regularizes” apparent nonergodicity emerging for FBM in the presence of stochastic resetting [33,48].

Note that the theoretically desirable rescaling (25) might not always be realizable in SPT experiments, performed, e.g., for an ensemble of mass-polydisperse tracers. Certain restrictions of measurement protocols and limitations of the apparatus itself (in terms of recording time, measurement precision, etc.) can prevent such an idealized scenario from happening. As a result, nonrescaled EB parameter will be extracted from the SPT time series. We therefore presented the main theoretical results for variation of the EB parameter of massive FBM and pronounced emerging nonergodicity in such a practice-related setup.

The nonergodicity of underdamped FBM is therefore “apparent,” being the direct consequence of insufficient trajectory lengths for progressively heavier particles (the time, required to visit cells in the phase-space in the same proportion as lighter particles, to attain a similar degree of ergodicity). This is similar to the “apparent” nonergodicity predicted, e.g., in a two-state switching-diffusion model [49] [with, respectively, $\{k_1, D_1\}$ and $\{k_2, D_2\}$ being the switching rates and diffusivities]. Such a model (see also Refs. [50,51]) becomes “apparently” profoundly nonergodic when the mean resident time in a given diffusion state exceeds the overall length of the trajectory (i.e., for occupation times [49] $\tau_{1,2} = 1/k_{1,2} \gtrsim T$).

Note here also that above we followed the definitions of the MSD and TAMSD standard for the SPT-data analysis [45–47,52–54], although some alternative “next-level” definitions of (non-)ergodicity can (in some situations) be

theoretically more appropriate for assessing the MSD-versus-TAMSD equivalence (see, e.g., Refs. [55–57]).

Finally, this analysis continues a series of recent studies of (non-)ergodic dynamics of massive particles for anomalous-diffusion processes with a power-law $D(t)$ [41,42,58] and exponential and logarithmic forms of $D(t)$ [59]. The extension of the “nonzero-mass concept” for unveiling the MSD-versus-TAMSD nonequivalence and EB-based nonergodicity is of interest also for other models of anomalous diffusion [4,6,24,60–63], for both pure and “modified” processes (e.g., by external confinement [9,64], TAMSD-aging effects [42,65], diffusion in barrier-escape setups [66], and for stochastic-resetting protocols [33,48]).

IV. ABBREVIATIONS

Brownian motion, BM; fractional BM, FBM; mean-squared displacement, MSD; time-averaged MSD, TAMSD; Ornstein-Uhlenbeck, OU; single-particle tracking, SPT.

ACKNOWLEDGMENTS

A.G.C. gratefully acknowledges the Humboldt University of Berlin for hospitality and support. R.M. acknowledges financial support by Deutsche Forschungsgemeinschaft (DFG Grant ME 1535/12-1). R.M. thanks the Foundation for Polish Science (Fundacja na rzecz Nauki Polskiej) for support within an Alexander von Humboldt Polish Honorary Research Scholarship.

APPENDIX A: DERIVATION OF THE MSD, MEAN TAMSD, AND EB FOR MASSIVE FBM

1. MSD

a. General solution

The Langevin-type equation of a single massive-FBM particle of mass m can be written as

$$m d^2 x(t)/dt^2 = -\gamma dx(t)/dt + \gamma \eta_H(t), \quad (\text{A1})$$

where γ is the damping coefficient. In the overdamped limit, the inertia term in (A1) can be neglected yielding the massless-FBM formulation [2,7–9,13]. The external-noise intensity, scaling as $\propto K_{2H}^{1/2}$ as per Eq. (2), is generally not coupled to the friction coefficient. With the velocity

$$dx(t)/dt = v(t) \quad (\text{A2})$$

Eq. (A1) is the velocity-OU process [44] for $v(t)$ driven by fractional Gaussian noise η_H with the correlator (2), i.e.,

$$dv(t)/dt = -\tau_0^{-1}v(t) + \tau_0^{-1}\eta_H(t). \quad (\text{A3})$$

Here $\tau_0 = m/\gamma$ is the velocity-relaxation time (11). The formal solution of Eq. (A3) with the initial condition $v(t=0) = v_0$ is

$$v(t) = v_0 e^{-t/\tau_0} + e^{-t/\tau_0} \int_0^t e^{t'/\tau_0} \tau_0^{-1} \eta_H(t') dt'. \quad (\text{A4})$$

The noise-averaged squared velocity is given by [56]

$$\begin{aligned} \langle v^2(t) \rangle &= e^{-2t/\tau_0} \left[v_0^2 + K_{2H} t^{2H} \tau_0^{-2} \mathcal{M}(2H, 2H+1, t/\tau_0) \right] \\ &+ 2HK_{2H} \tau_0^{2H-2} \gamma(2H, t/\tau_0), \end{aligned} \quad (\text{A5})$$

where $B_H(t)$ is FBM, $\mathcal{M}(a, b, z)$ is the confluent hypergeometric (or the Kummer’s) function of the first kind,

$$\mathcal{M}(a, b, z) = \frac{\Gamma(b)}{\Gamma(b-a)\Gamma(a)} \int_0^1 e^{zt} t^{a-1} (1-t)^{b-a-1} dt, \quad (\text{A6})$$

and $\gamma(a, z)$ is the lower incomplete Gamma function,

$$\gamma(a, z) = \int_0^z e^{-x} x^{a-1} dx. \quad (\text{A7})$$

The expression (A5) follows from Eq. (28) of Ref. [56] [see also the detailed derivation there] after setting the relaxation time to τ_0 and the actual noise strength as in Eq. (A3), after some algebra with the \mathcal{M} -functions [67].

b. Short- and long-time limits

At short times, when

$$\{t, \Delta\} \ll \tau_0, \quad (\text{A8})$$

using the small-argument expansions $\mathcal{M}(2H, 2H+1, t/\tau_0) \approx 1$ and $\gamma(2H, t/\tau_0) \approx (2H)^{-1}(t/\tau_0)^{2H}$, one gets from (A5) that

$$\langle v^2(t) \rangle \approx v_0^2 + 2K_{2H} \tau_0^{-2} t^{2H}, \quad (\text{A9})$$

whereas at long times, at

$$t \gg \tau_0, \quad (\text{A10})$$

using the respective expansions $\mathcal{M}(2H, 2H+1, t/\tau_0) \approx 2H e^{t/\tau_0} (t/\tau_0)^{-1}$ and $\gamma(2H, t/\tau_0) \approx \Gamma(2H)$, where $\Gamma(x)$ is the Gamma function, we find stationary, time-independent velocities of the particles in the parabolic OU potential. The long-time, stationary-state-related mean-squared velocity $\langle v^2(t) \rangle$ follows then from (A5) as

$$\langle v^2(t) \rangle \approx \langle v^2 \rangle_{\text{st}} = K_{2H} \tau_0^{2H-2} \Gamma(2H+1). \quad (\text{A11})$$

The Gaussian distribution of long-time velocities,

$$p_{\text{st}}(v) = \exp\left(-\frac{v^2}{2\langle v^2 \rangle_{\text{st}}}\right) / \sqrt{2\pi \langle v^2 \rangle_{\text{st}}}, \quad (\text{A12})$$

is akin to the one-dimensional Maxwell-Boltzmann distribution with effective H -dependent temperature defined as

$$\mathcal{T}_{\text{eff}}(H) = m \langle v^2 \rangle_{\text{st}} / k_B, \quad (\text{A13})$$

where k_B is the Boltzmann constant. For this *nonequilibrium* system the width of $p_{\text{st}}(v)$ in (A12) and the mean-squared velocity $\langle v^2 \rangle_{\text{st}}$ given by (A11) can thus be expressed via $\mathcal{T}_{\text{eff}}(H)$ [no equipartition theorem or fluctuation-dissipation relation is connected to \mathcal{T}_{eff} (A13)]. The distribution (A12) satisfies the stationary Fokker-Planck equation for the fractional velocity-OU process (A3) given by [68,69]

$$\langle v^2 \rangle_{\text{st}} \partial^2 p_{\text{st}}(v) / \partial v^2 + \partial [v p_{\text{st}}(v)] / \partial v = 0. \quad (\text{A14})$$

The asymptotic result for the velocity-autocorrelation function of the fractional OU process for the stationary velocities for the well-separated time instances, at $\delta t \gg \tau_0$, is given by [56] (see also Ref. [70])

$$\langle v(t)v(t+\delta t) \rangle \approx K_{2H} 2H(2H-1)(\delta t)^{2H-2}, \quad (\text{A15})$$

while at $\delta t \ll \tau_0$ we have

$$\langle v(t)v(t + \delta t) \rangle \approx \langle v^2 \rangle_{\text{st}}. \quad (\text{A16})$$

As m , γ , and noise strength are independent model parameters, to get simpler solutions and to capture main physical scalings, we consider now the “large-mass” or “short-trajectory” limit of Eq. (A3) via setting τ_0 to a large value, but such that the product $\tau_0^{-1}K_{2H}^{1/2}$ stays constant via adjusting the noise strength [neglecting, thus, the second term in (A3)]. The evolution of velocity at short times, starting from v_0 value, is then simply integrated $\eta_H(t)$ that is FBM, namely,

$$v(t) \approx v_0 + \tau_0^{-1} \int_0^t \eta_H(t') dt' = v_0 + \tau_0^{-1} B_H(t). \quad (\text{A17})$$

The velocity-autocorrelation function and the velocity second moment are then given, respectively, by

$$\langle v(t')v(t'') \rangle \approx v_0^2 + \tau_0^{-2} \langle B_H(t')B_H(t'') \rangle \quad (\text{A18})$$

and

$$\langle v^2(t) \rangle \approx v_0^2 + 2K_{2H}\tau_0^{-2}t^{2H}. \quad (\text{A19})$$

As per Eq. (A2), the particle position $x(t)$ is one more integration of (A17), the MSD in this limit for the initial condition $x(t=0) = 0$ is a combination of a ballistic $\sim t^2$ and a faster-than-ballistic $\sim t^{2H+2}$ term, namely,

$$\langle x^2(t) \rangle \approx v_0^2 t^2 + 2K_{2H}\tau_0^{-2}(2H+2)^{-1}t^{2H+2}. \quad (\text{A20})$$

c. Distributed v_0 velocities

Assuming initial velocities to be distributed with the stationary-state distribution (A12), the MSD at short times—after neglecting the second term in (A20)—reads

$$\langle x^2(t) \rangle \approx \langle v^2 \rangle_{\text{st}} t^2, \quad (\text{A21})$$

while at long times (A10) one gets

$$\langle x^2(t) \rangle \approx 2K_{2H}t^{2H}. \quad (\text{A22})$$

We note that the long-time MSD behavior is observed beyond the transition time t_{MSD}^* scaling as [via equating the second term in (A20) and (A22)]

$$t_{\text{MSD}}^*/\tau_0 \sim (2H+2)^{1/2} \quad (\text{A23})$$

and [via comparing (A21) and (A22)]

$$(t_{\text{MSD}}^*/\tau_0)|_{\text{stat. } v_0} \sim [\Gamma(2H+1)/2]^{1/(2H-2)} \quad (\text{A24})$$

for the case of $v_0 = 0$ and $p_{\text{st}}(v_0)$ -distributed initial velocities of the particles, correspondingly. For a (vanishingly) small mass, neglecting the first term in Eq. (A3), one gets the expected MSD of massless FBM,

$$\langle x^2(t) \rangle \approx 2K_{2H}t^{2H}. \quad (\text{A25})$$

2. TAMSD

a. Short-time limit

For the TAMSD (5), formally integrating expression (A2) from t to $t + \Delta$, we get

$$\overline{\delta^2(\Delta)} = \frac{1}{T-\Delta} \int_0^{T-\Delta} \left[\int_t^{t+\Delta} v(t') dt' \right]^2 dt. \quad (\text{A26})$$

For the region of short lag times, when (A8) holds, neglecting the variation of velocity $v(t)$ on the timescale of Δ , we find from (A26) that

$$\overline{\delta^2(\Delta)} \approx \overline{\delta_{\text{app}}^2(\Delta)} \equiv \frac{\Delta^2}{T-\Delta} \int_0^{T-\Delta} \langle v^2(t) \rangle dt. \quad (\text{A27})$$

For short trajectories or large particle mass, i.e., at

$$T \ll \tau_0, \quad (\text{A28})$$

when velocities did not yet reach stationarity, after using the approximate velocity (A9) the TAMSD form (A27) yields—similarly to the MSD representation (A20)—a combination of two terms,

$$\overline{\delta^2(\Delta)} \approx v_0^2 \Delta^2 + 2K_{2H}(2H+1)^{-1}(T-\Delta)^{2H}(\Delta/\tau_0)^2, \quad (\text{A29})$$

both featuring a ballistic TAMSD growth at $T \gg \Delta$.

b. Long-time limit

For long trajectories, when

$$T \gg \tau_0, \quad (\text{A30})$$

and, thus, for nearly stationary particle velocities, we split the integral in (A27) into two regions, with $0 < t < \tau_0$ and $\tau_0 < t < (T-\Delta)$. In the first region we use the short-time expansion of $\langle v^2(t) \rangle$ near v_0^2 given by (A19), while in the other region the long-time result (A11) with $\langle v^2(t) \rangle \approx \langle v^2 \rangle_{\text{st}}$ is used. With this strategy, after integration, the approximate mean TAMSD in this limit becomes

$$\overline{\delta^2(\Delta)} \approx \frac{\tau_0 \Delta^2}{T-\Delta} \left[v_0^2 + 2K_{2H}(2H+1)^{-1} \tau_0^{2H-2} + K_{2H} \Gamma(2H+1)(T-\Delta-\tau_0) \tau_0^{2H-3} \right]. \quad (\text{A31})$$

From this expression, neglecting the duration of Δ and τ_0 compared to the trace length T , one gets the expected short-lag-time ballistic scaling,

$$\overline{\delta^2(\Delta)} \approx K_{2H} \tau_0^{2H} \Gamma(2H+1) (\Delta/\tau_0)^2 = \langle v^2 \rangle_{\text{st}} \Delta^2. \quad (\text{A32})$$

This asymptotic TAMSD is identical to the MSD evolution under the same conditions, Eq. (A22). Therefore, the ergodicity in terms of MSD-to-TAMSD equivalence at short lag times is restored for long trajectories and stationary-state velocities.

When both the measurement time and the lag time are longer than the velocity-relaxation timescale, i.e., at $\tau_0 \ll \{\Delta, T\}$, after using the correlator

$$\langle v(t')v(t'') \rangle = \langle \eta_H(t')\eta_H(t'') \rangle, \quad (\text{A33})$$

following from Eq. (1) with the initial velocities being fully relaxed by that long time, for the mean TAMSD—starting from expression (A26) and performing the elementary integration—we find

$$\overline{\delta^2(\Delta)} = 2K_{2H} \Delta^{2H}. \quad (\text{A34})$$

The MSD-to-TAMSD equivalence is thus again restored. The transition lag time from the short-time TAMSD behavior

(A32) to the long-time asymptotic law (A34), denoted as Δ_{TAMSD}^* , is the same as that for the MSD case with stationary-state-distributed v_0 given by (A24),

$$(\Delta_{\text{TAMSD}}^*/\tau_0) = (\Delta_{\text{MSD}}^*/\tau_0)|_{\text{stat.}v_0}. \quad (\text{A35})$$

3. EB

The standard procedure for computing the EB parameter is to find the general expression for the fourth-order correlation functions of particle positions (for Gaussian random variables) and with its help express all nine terms in the integrand of the fourth-moment $\langle (\delta^2(\Delta))^2 \rangle$ in EB in Eq. (8). This general methodology is often tedious (we refer, e.g., to EB of the OU process computed like this in Ref. [71]). Our goal here is—via avoiding exact lengthy derivations—that are not easy to use in practice, i.e., because of special functions often involved that demand a considerable time to find relevant scalings—to derive EB of massive FBM approximately and get the main relevant scaling relations.

a. Short-time limit

To pursue this goal, for the region of short lag times defined by (A8), using the approximate TAMSD $\langle \delta_{\text{app}}^2(\Delta) \rangle$ in (A27) and employing Isserlis-Wick theorem for zero-mean Gaussian processes,

$$\begin{aligned} & \langle v(t')v(t'')v(t''')v(t''''') \rangle \\ &= \langle v(t')v(t'') \rangle \langle v(t''')v(t''''') \rangle + \langle v(t')v(t''') \rangle \langle v(t'')v(t''''') \rangle \\ &+ \langle v(t')v(t''''') \rangle \langle v(t'')v(t''') \rangle, \end{aligned} \quad (\text{A36})$$

for computing the fourth-order correlators in terms of the pair correlators in Eq. (8), EB of massive FBM for short trajectories or large particle mass can be approximated as

$$\begin{aligned} \text{EB}(\Delta) &\approx \frac{\int_0^{T-\Delta} dt' \int_0^{T-\Delta} dt'' \langle v^2(t')v^2(t'') \rangle}{\left[\int_0^{T-\Delta} dt' \langle v^2(t') \rangle \right]^2} - 1 \\ &= \frac{2 \int_0^{T-\Delta} dt' \int_0^{T-\Delta} dt'' \langle v(t')v(t'') \rangle^2}{\left[\int_0^{T-\Delta} dt' \langle v^2(t') \rangle \right]^2}. \end{aligned} \quad (\text{A37})$$

Using the velocity-velocity correlator (A18), the FBM autocorrelation function

$$\langle B_H(t')B_H(t'') \rangle = K_{2H}[(t')^{2H} + (t'')^{2H} - |t' - t''|^{2H}] \quad (\text{A38})$$

and setting

$$v_0 = 0, \quad (\text{A39})$$

for short- T or large- m values [when the condition (A28) holds] the integrand in the nominator of (A37) becomes

$$\begin{aligned} \langle v(t')v(t'') \rangle^2 &= \tau_0^{-4} K_{2H}^2 [(t')^{4H} + (t'')^{4H} + 2(t')^{2H}(t'')^{2H} \\ &- 2(t')^{2H}|t' - t''|^{2H} - 2(t'')^{2H}|t' - t''|^{2H} + |t' - t''|^{4H}]. \end{aligned} \quad (\text{A40})$$

With this result, taking the elementary integrals in (A37), using the symmetry with respect to swapping $t' \leftrightarrow t''$ in the

integrals, and employing that

$$\begin{aligned} & \int_0^{T-\Delta} dt' \left[\int_0^{T-\Delta} dt'' 2(t')^{2H} |t' - t''|^{2H} \right] = (T - \Delta)^{4H+2} \\ & \times \left[\frac{1}{(2H+1)^2} + \frac{2}{2H+1} \frac{\Gamma(2H+1)\Gamma(2H+2)}{\Gamma(4H+3)} \right], \end{aligned} \quad (\text{A41})$$

the EB parameter in this limit has *no dependence* on the lag time and attains the H -dependent value

$$\text{EB} \approx \frac{2H+1}{2} \left[\frac{4H+3}{4H+1} - 4 \frac{\Gamma(2H+1)\Gamma(2H+2)}{\Gamma(4H+3)} \right]. \quad (\text{A42})$$

The values of EB (A42) for a set of typical Hurst exponents $H = \{0, \frac{1}{4}, \frac{1}{2}, \frac{3}{4}, 1\}$ are as follows: $\text{EB} = \{\frac{1}{2}, \frac{3}{4}(2 - \frac{\pi}{4}), \frac{4}{3}, \frac{5}{4}(\frac{3}{2} - \frac{3\pi}{64}), 2\}$. The results of computer simulations for large particle mass for zero initial velocities $v_0 = 0$ (the EBs on the right side of Fig. 3) are in excellent agreement with (A42), see also Fig. 9.

For initial velocities v_0 distributed with the stationary-state distribution $p_{\text{st}}(v_0)$ given by Eq. (A12), the same strategy of EB computation in the short-time or large-mass limit can be employed. Specifically, we start with the general EB form (A37) and use the second moment (A19) and the autocorrelation function (A18) with

$$\langle v_0^2 \rangle = \langle v^2 \rangle_{\text{st}} \quad (\text{A43})$$

given by (A11). The double angular brackets denote averaging over realizations of initial velocities. After integration, the nominator of EB in Eq. (A37) becomes

$$\begin{aligned} & 2 \int_0^{T-\Delta} dt' \int_0^{T-\Delta} dt'' \langle v(t')v(t'') \rangle^2 \\ &= 2K_{2H}^2 \tau_0^{-4} \left\{ [\Gamma(2H+1)]^2 \tau_0^{4H} (T-\Delta)^2 + 4\Gamma(2H+1) \right. \\ &\times \tau_0^{2H} (2H+2)^{-1} (T-\Delta)^{2H+2} + (T-\Delta)^{4H+2} \\ &\times \left[\frac{4H+3}{(4H+1)(2H+1)} \right. \\ &\left. \left. - \frac{4}{2H+1} \frac{\Gamma(2H+1)\Gamma(2H+2)}{\Gamma(4H+3)} \right] \right\}, \end{aligned} \quad (\text{A44})$$

while the denominator is given by

$$\begin{aligned} & \left[\int_0^{T-\Delta} dt' \langle v^2(t') \rangle \right]^2 = K_{2H}^2 \tau_0^{-4} \left\{ [\Gamma(2H+1)]^2 \tau_0^{4H} (T-\Delta)^2 \right. \\ &+ 4\Gamma(2H+1) \tau_0^{2H} (2H+1)^{-1} (T-\Delta)^{2H+2} \\ &+ 4(2H+1)^{-2} (T-\Delta)^{4H+2} \}. \end{aligned} \quad (\text{A45})$$

In the limit of large mass or short traces, at $T/\tau_0 \ll 1$, the highest powers of τ_0 in these expressions dominate yielding in the leading order

$$\text{EB}(\Delta) \approx 2 \quad (\text{A46})$$

for all values of the Hurst exponent H . The value (A46) is shown as the large-mass EB plateau in Fig. 10 and several

other EB plots. Note that for particles of large mass in the scenario $v_0 = 0$ the EB values are H -dependent as given by (A42), while for the initial velocities obeying the stationary distribution (A12) the ergodicity-breaking parameter in this limit approaches $EB = 2$ as per (A46); compare the large-mass EB values of Figs. 3 and 10.

b. Long-time limit

At long measurement times, when (A30) is valid, the velocities executing the fractional OU process are stationary, $\langle v^2(t) \rangle \rightarrow \langle v^2 \rangle_{st}$. Starting from the representation (A37), the leading-order approximation of EB is

$$EB(\Delta) \approx 4 \frac{\int_0^{T-\Delta} \langle v(t_1)v(t_2) \rangle^2 |_{\tau=|t_1-t_2|} d\tau}{\langle v^2 \rangle_{st}^2 (T-\Delta)}. \quad (\text{A47})$$

The velocity-autocorrelation features different forms for $\tau \ll \tau_0$ given by (A15) and for $\tau \gg \tau_0$ in Eq. (A16). Similarly to the approximate TAMSD evaluation in the long-time limit in (A31), we split the integral in expression (A47) into two parts, utilize these different velocity-velocity correlators, and get

$$EB(\Delta) \approx 4 \frac{\int_0^{\tau_0} \langle v^2 \rangle_{st}^2 d\tau + \int_{\tau_0}^{T-\Delta} d\tau [K_{2H} 2H(2H-1)\tau^{2H-2}]^2}{\langle v^2 \rangle_{st}^2 (T-\Delta)}. \quad (\text{A48})$$

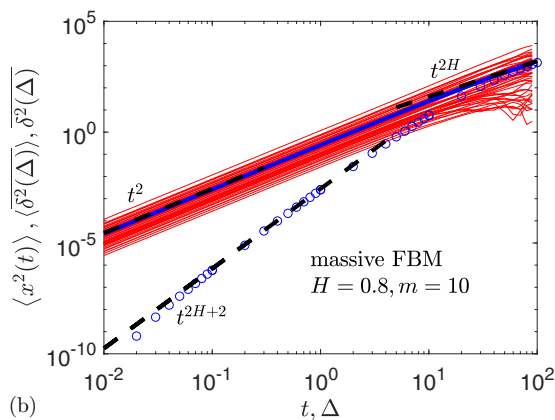
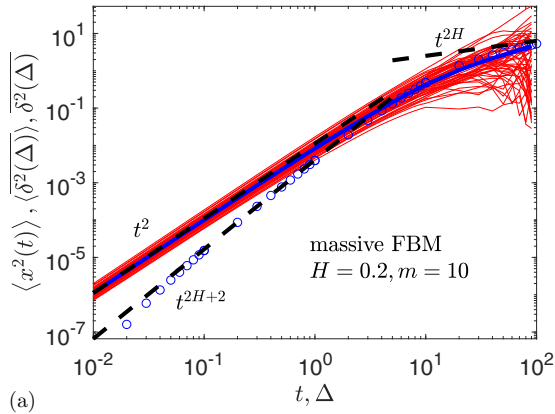


FIG. 5. The same as in Fig. 1, for the same parameters and with the same asymptotes being shown, except for heavier particles, with $m = 10$. The initial velocities are $v_0 = 0$.

After elementary integration, neglecting the terms of order $\Delta/T \ll 1$, the value of EB becomes independent on the lag time, obeying the relation

$$EB \approx 4\tau_0/T + C_3(H)[(\tau_0/T)^{4-4H} - \tau_0/T], \quad (\text{A49})$$

where the coefficient C_3 reads (see Fig. 11 for its variation)

$$C_3(H) = \frac{16H^2(2H-1)^2}{[\Gamma(2H+1)]^2(4H-3)}. \quad (\text{A50})$$

In EB expression (A49), the lag time Δ is effectively replaced by the characteristic timescale τ_0 . At $\tau_0/T \ll 1$, after retaining the leading-order terms in (A49), one gets [similarly to the two-region solution for EB of massless FBM given by Eq. (23)] the following scaling relations

$$EB \approx \begin{cases} [4 - C_3(H)] \times (\tau_0/T)^1, & 0 < H < 3/4 \\ C_3(H) \times (\tau_0/T)^{4-4H}, & 1 > H > 3/4 \end{cases} \quad (\text{A51})$$

As $\tau_0 = m/\gamma$, the relations (23) and (24)—used to rationalize the simulation data for $EB(\Delta_1, T, m)$ obtained for varying trace length T and particle mass m —instantly follow from Eq. (A51).

As a next-order approximation, instead of (A16) we use the small-increment expansion in the stationary regime

$$\langle v(t)v(t+\delta t) \rangle \approx \langle v^2 \rangle_{st} - K_{2H}\tau_0^{-2}(\delta t)^{2H}, \quad (\text{A52})$$

while for the well-separated increments (A15) is still employed. Then, repeating the calculations starting from the EB expression (A48), one gets the same scalings as in

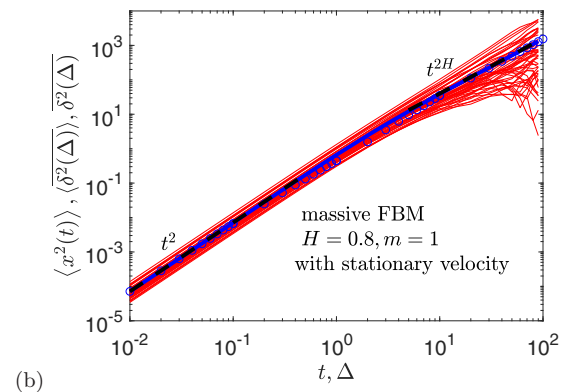
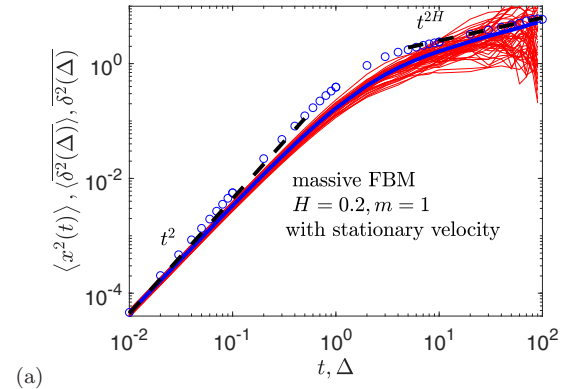


FIG. 6. The same as in Fig. 1, for the same model parameters, except for initial velocities taken from the stationary distribution $p_{st}(v_0)$ given by (A12).

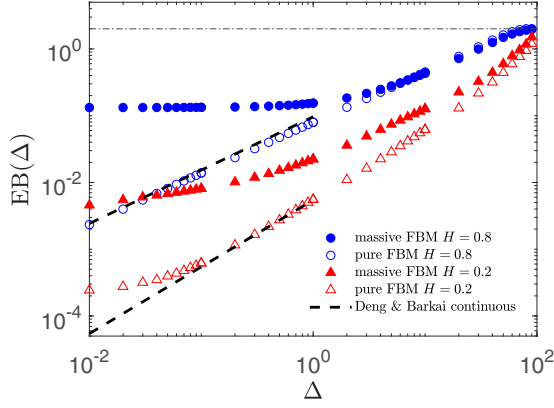


FIG. 7. EB parameter (8) plotted versus lag time Δ for two values of the Hurst H exponent (see the legend). The theoretical continuous-time asymptote (18) by Deng-Barkai [7] and the terminal EB value (22) are the dashed and dot-dashed black lines, respectively. The initial velocities are $v_0 = 0$. Parameters: $T = 10^2$, $dt = 10^{-2}$.

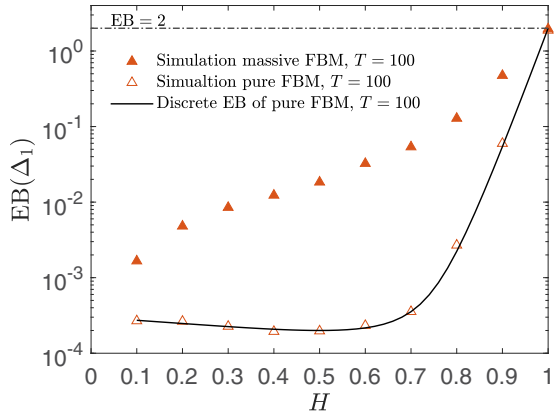


FIG. 8. Variation of $EB(\Delta_1)$ of overdamped FBM from the simulation data (as those in Fig. 7) versus the Hurst exponent H . The prediction of the discrete-time theory of EB for massless FBM [13,31] given by (21) is also shown (see the legend). The initial velocity is $v_0 = 0$. Parameters: $m = 1$, $T = 10^2$, and $\Delta_1 = dt = 10^{-2}$.

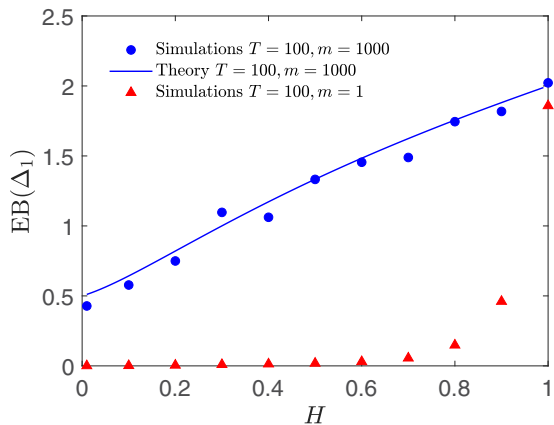


FIG. 9. EB parameter of massive FBM in the limit $T \ll m/\gamma = \tau_0$ (the blue symbols) and $T \gg \tau_0$ (the red symbols, see the legend). The analytical short-trace or large-mass EB asymptote given by expression (A42) is the solid blue curve for the case $T \ll \tau_0$. The initial velocity is $v_0 = 0$.

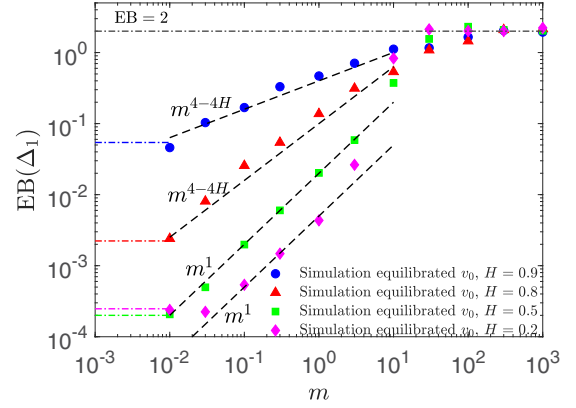


FIG. 10. The same as in Fig. 3, for the same parameters and with scaling relations (23) shown, but computed for initial velocities distributed as in the stationary state, with $p_{st}(v_0)$ given by (A12). The large-mass-asymptote (A46) is the dot-dashed black line at $EB=2$.

(A51), but with the improved coefficient for $0 < H < 3/4$, namely,

$$EB \approx \begin{cases} [4 - C_4(H)] \times (\tau_0/T)^1, & 0 < H < 3/4 \\ C_3(H) \times (\tau_0/T)^{4-4H}, & 1/2 > H > 3/4 \end{cases} \quad (\text{A53})$$

where

$$C_4(H) = C_3(H) + \frac{8}{\Gamma(2H+2)} - \frac{4}{[\Gamma(2H+1)]^2(4H+1)}. \quad (\text{A54})$$

The variation of coefficients $C_3(H)$ and $C_4(H)$ with the Hurst exponent H is shown for completeness in Fig. 11. Using a more accurate Eq. (A53) instead of (A51) enables a *quantitative* description of the EB-versus- m data extracted from simulations, as shown in Fig. 3.

APPENDIX B: AUXILIARY FIGURES

Here we present some auxiliary figures (Figs. 5–11) supporting the claims of the main text.

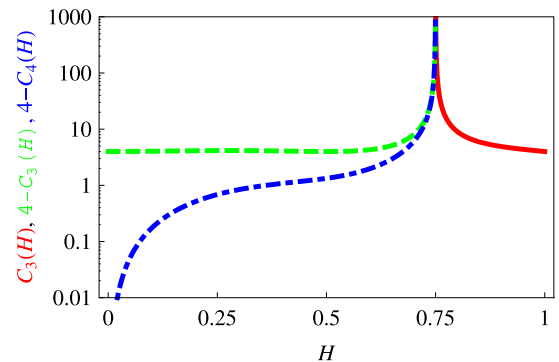


FIG. 11. Prefactors in expressions (A51) and (A54), with a visible divergence at the “critical” Hurst exponent $H = 3/4$. The coefficients $C_3(H)$, $4 - C_3(H)$, and $4 - C_4(H)$ are denoted by the solid red, the dashed green, and the dot-dashed blue curves, respectively.

- [1] A. N. Kolmogorov, Wiener'sche Spiralen und einige andere interessante Kurven im Hilbertschen Raum, *C. R. (Doklady) Acad. Sci. URSS (N.S.)* **26**, 115 (1940).
- [2] B. B. Mandelbrot and J. W. van Ness, Fractional Brownian motions, fractional noises and applications, *SIAM Rev.* **10**, 422 (1968).
- [3] S. Burov, J.-H. Jeon, R. Metzler, and E. Barkai, Single particle tracking in systems showing anomalous diffusion: The role of weak ergodicity breaking, *Phys. Chem. Chem. Phys.* **13**, 1800 (2011).
- [4] I. M. Sokolov, Models of anomalous diffusion in crowded environments, *Soft Matter* **8**, 9043 (2012).
- [5] F. Höfling and T. Franosch, Anomalous transport in the crowded world of biological cells, *Rep. Prog. Phys.* **76**, 046602 (2013).
- [6] R. Metzler, J.-H. Jeon, A. G. Cherstvy, and E. Barkai, Anomalous diffusion models and their properties: Non-stationarity, non-ergodicity, and ageing at the centenary of single particle tracking, *Phys. Chem. Chem. Phys.* **16**, 24128 (2014).
- [7] W. Deng and E. Barkai, Ergodic properties of fractional Brownian-Langevin motion, *Phys. Rev. E* **79**, 011112 (2009).
- [8] J.-H. Jeon and R. Metzler, Fractional Brownian motion and motion governed by the fractional Langevin equation in confined geometries, *Phys. Rev. E* **81**, 021103 (2010).
- [9] J.-H. Jeon and R. Metzler, Inequivalence of time and ensemble averages in ergodic systems: Exponential versus power-law relaxation in confinement, *Phys. Rev. E* **85**, 021147 (2012).
- [10] S. Vitali, V. Sposini, O. Sliusarenko, P. Paradisi, G. Castellani, and G. Pagnini, Langevin equation in complex media and anomalous diffusion, *J. R. Soc., Interface* **15**, 20180282 (2018).
- [11] F. Thiel and I. M. Sokolov, Weak ergodicity breaking in an anomalous diffusion process of mixed origins, *Phys. Rev. E* **89**, 012136 (2014).
- [12] M. Schwarzl, A. Godec, and R. Metzler, Quantifying non-ergodicity of anomalous diffusion with higher order moments, *Sci. Rep.* **7**, 3878 (2017).
- [13] W. Wang, A. G. Cherstvy, A. V. Chechkin, S. Thapa, F. Seno, X. Liu, and R. Metzler, Fractional Brownian motion with random diffusivity: Emerging residual nonergodicity below the correlation time, *J. Phys. A* **53**, 474001 (2020).
- [14] J. L. Lebowitz and O. Penrose, Modern ergodic theory, *Phys. Today* **26(2)**, 23 (1973).
- [15] J.-P. Bouchaud, Weak ergodicity breaking and aging in disordered systems, *J. Phys. I* **2**, 1705 (1992).
- [16] G. Bel and E. Barkai, Weak Ergodicity Breaking in the Continuous-Time Random Walk, *Phys. Rev. Lett.* **94**, 240602 (2005).
- [17] C. C. Moore, Ergodic theorem, ergodic theory, and statistical mechanics, *Proc. Natl. Acad. Sci. USA* **112**, 1907 (2015).
- [18] G. W. Mackey, Ergodic theory and its significance for statistical mechanics and probability theory, *Adv. in Mathematics* **12**, 178 (1974).
- [19] O. Penrose, Foundations of statistical mechanics, *Rep. Prog. Phys.* **42**, 1937 (1979).
- [20] G. Gallavotti, Ergodicity, ensembles, irreversibility in Boltzmann and beyond, *J. Stat. Phys.* **78**, 1571 (1995).
- [21] P. B. M. Vranas, Epsilon-ergodicity and the success of equilibrium statistical mechanics, *Philos. Sci.* **65**, 688 (1998).
- [22] Y. Lanoiselee and D. S. Grebenkov, Revealing nonergodic dynamics in living cells from a single particle trajectory, *Phys. Rev. E* **93**, 052146 (2016).
- [23] H. Loch-Olszewska, G. Sikora, and J. Janczura, Identifying ergodicity breaking for fractional anomalous diffusion: Criteria for minimal trajectory length, *Phys. Rev. E* **94**, 052136 (2016).
- [24] A. Weron and M. Magdziarz, Generalization of the Khinchin Theorem to Lévy Flights, *Phys. Rev. Lett.* **105**, 260603 (2010).
- [25] Y. He, S. Burov, R. Metzler, and E. Barkai, Random Time-Scale Invariant Diffusion and Transport Coefficients, *Phys. Rev. Lett.* **101**, 058101 (2008).
- [26] R. D. Mountain and D. Thirumalai, Measures of effective ergodic convergence in liquids, *J. Phys. Chem.* **93**, 6975 (1989).
- [27] D. Thirumalai, R. D. Mountain, and T. R. Kirkpatrick, Ergodic behavior in supercooled liquids and in glasses, *Phys. Rev. A* **39**, 3563 (1989).
- [28] D. Thirumalai and R. D. Mountain, Ergodic convergence properties of supercooled liquids and glasses, *Phys. Rev. A* **42**, 4574 (1990).
- [29] W. Wang, A. G. Cherstvy, X. Liu, and R. Metzler, Anomalous diffusion and nonergodicity for heterogeneous diffusion processes with fractional Gaussian noise, *Phys. Rev. E* **102**, 012146 (2020).
- [30] A. Andreev and D. S. Grebenkov, Time-averaged MSD of Brownian motion, *J. Stat. Mech.* (2012) P07001.
- [31] D. S. Grebenkov, Optimal and suboptimal quadratic forms for noncentered Gaussian processes, *Phys. Rev. E* **88**, 032140 (2013).
- [32] E. Geneston, R. Tuladhar, M. T. Beig, M. Bologna, and P. Grigolini, Ergodicity breaking and localization, *Phys. Rev. E* **94**, 012136 (2016).
- [33] W. Wang, A. G. Cherstvy, H. Kantz, R. Metzler, and I. M. Sokolov, Time-averaging and emerging nonergodicity upon resetting of fractional Brownian motion and heterogeneous diffusion processes, *Phys. Rev. E* **104**, 024105 (2021).
- [34] T. Franosch, M. Grimm, M. Belushkin, F. M. Mor, G. Foffi, L. Forro, and S. Jeney, Resonances arising from hydrodynamic memory in Brownian motion, *Nature (London)* **478**, 85 (2011).
- [35] R. Huang, I. Chavez, K. M. Taute, B. Lukic, S. Jeney, M. G. Raizen, and E.-L. Florin, Direct observation of the full transition from ballistic to diffusive Brownian motion in a liquid, *Nat. Phys.* **7**, 576 (2011).
- [36] T. Li and M. G. Raizen, Brownian motion at short time scales, *Ann. Phys. (Berlin)* **525**, 281 (2013).
- [37] J. Duplat, S. Kheifets, T. Li, M. G. Raizen, and E. Villermaux, Superdiffusive trajectories in Brownian motion, *Phys. Rev. E* **87**, 020105(R) (2013).
- [38] S. Kheifets, A. Simha, K. Melin, T. Li, and M. G. Raizen, Observation of Brownian motion in liquids at short times: Instantaneous velocity and memory loss, *Science* **343**, 1493 (2014).
- [39] K. Capala and B. Dybiec, Underdamped, anomalous kinetics in double-well potentials, *Phys. Rev. E* **102**, 052123 (2020).
- [40] N. Makris, Impulse response function for Brownian motion, *Soft Matter* **17**, 5410 (2021).
- [41] A. Bodrova, A. V. Chechkin, A. G. Cherstvy, H. Safdari, I. M. Sokolov, and R. Metzler, Underdamped scaled Brownian motion: (Non-)existence of the overdamped limit in anomalous diffusion, *Sci. Rep.* **6**, 30520 (2016).

- [42] H. Safdari, A. G. Cherstvy, A. V. Chechkin, A. Bodrova, and R. Metzler, Aging underdamped scaled Brownian motion: Ensemble- and time-averaged particle displacements, nonergodicity, and the failure of the overdamping approximation, *Phys. Rev. E* **95**, 012120 (2017).
- [43] J.-F. Coeurjolly, Simulation and identification of the fractional Brownian motion: A bibliographical and comparative study, *J. Stat. Softw.* **5**, 1 (2000).
- [44] G. E. Uhlenbeck and L. S. Ornstein, On the theory of the Brownian motion, *Phys. Rev.* **36**, 823 (1930).
- [45] S. Thapa, M. A. Lomholt, J. Krog, A. G. Cherstvy, and R. Metzler, Bayesian nested-sampling analysis of single-particle tracking data: Maximum likelihood for the models of stochastic diffusivity and fractional Brownian motion, *Phys. Chem. Chem. Phys.* **20**, 29018 (2018).
- [46] A. G. Cherstvy, S. Thapa, C. E. Wagner, and R. Metzler, Non-Gaussian, non-ergodic, and non-Fickian diffusion of tracers in mucin hydrogels, *Soft Matter* **15**, 2526 (2019).
- [47] A. D. Fernandez, P. Charchar, A. G. Cherstvy, R. Metzler, and M. F. Finnis, The diffusion of doxorubicin drug molecules in silica nanoslits is non-Gaussian, intermittent and anticorrelated, *Phys. Chem. Chem. Phys.* **22**, 27955 (2020).
- [48] W. Wang, A. G. Cherstvy, R. Metzler, and I. M. Sokolov, Resetting massive fractional Brownian motion (unpublished).
- [49] D. S. Grebenkov, Time-averaged MSD for switching diffusion, *Phys. Rev. E* **99**, 032133 (2019).
- [50] T. Uneyama, T. Miyaguchi, and T. Akimoto, Fluctuation analysis of time-averaged mean-square displacement for the Langevin equation with time-dependent and fluctuating diffusivity, *Phys. Rev. E* **92**, 032140 (2015).
- [51] T. Miyaguchi, T. Akimoto, and E. Yamamoto, Langevin equation with fluctuating diffusivity: A two-state model, *Phys. Rev. E* **94**, 012109 (2016).
- [52] I. Golding and E. C. Cox, Physical Nature of Bacterial Cytoplasm, *Phys. Rev. Lett.* **96**, 098102 (2006).
- [53] M. Magdziarz, A. Weron, K. Burnecki, and J. Klafter, Fractional Brownian Motion Versus the Continuous-Time Random Walk: A Simple Test for Subdiffusive Dynamics, *Phys. Rev. Lett.* **103**, 180602 (2009).
- [54] K. Speckner and M. Weiss, Single-particle tracking reveals anti-persistent subdiffusion in cell extracts, *Entropy* **23**, 892 (2021).
- [55] R. Hou, A. G. Cherstvy, R. Metzler, and T. Akimoto, Biased continuous-time random walks for ordinary and equilibrium cases: Facilitation of diffusion, ergodicity breaking and ageing, *Phys. Chem. Chem. Phys.* **20**, 20827 (2018).
- [56] Y. Mardoukhi, A. V. Chechkin, and R. Metzler, Spurious ergodicity breaking in normal and fractional Ornstein–Uhlenbeck process, *New J. Phys.* **22**, 073012 (2020).
- [57] W. Wang, A. G. Cherstvy, R. Metzler, and I. M. Sokolov, Universal restoration of ergodicity for reset anomalous-diffusion processes (unpublished).
- [58] A. G. Cherstvy, and R. Metzler, Anomalous diffusion in time-fluctuating non-stationary diffusivity landscapes, *Phys. Chem. Chem. Phys.* **18**, 23840 (2016).
- [59] A. G. Cherstvy, H. Safdari, and R. Metzler, Anomalous diffusion, nonergodicity, and ageing for exponentially and logarithmically time-dependent diffusivity: Striking differences for massive versus massless particles, *J. Phys. D* **54**, 195401 (2021).
- [60] V. Zaboruaev, S. Denisov, and J. Klafter, Lévy walks, *Rev. Mod. Phys.* **87**, 483 (2015).
- [61] A. Bodrova, A. V. Chechkin, A. G. Cherstvy, and R. Metzler, Ultraslow scaled Brownian motion, *New J. Phys.* **17**, 063038 (2015).
- [62] O. Bénichou, P. Illien, G. Oshanin, A. Sarracino, and R. Voituriez, Diffusion and Subdiffusion of Interacting Particles on Comblike Structures, *Phys. Rev. Lett.* **115**, 220601 (2015).
- [63] C. Landim and S. B. Volchan, Equilibrium fluctuations for a driven tracer particle dynamics, *Stoch. Proc. Appl.* **85**, 139 (2000).
- [64] A. G. Cherstvy, A. V. Chechkin, and R. Metzler, Ageing and confinement in non-ergodic heterogeneous diffusion processes, *J. Phys. A* **47**, 485002 (2014).
- [65] A. G. Cherstvy and R. Metzler, Ergodicity breaking, ageing, and confinement in generalized diffusion processes with position and time dependent diffusivity, *J. Stat. Mech.* (2015) P05010.
- [66] O. Yu. Sliusarenko, V. Yu. Gonchar, A. V. Chechkin, I. M. Sokolov, and R. Metzler, Kramers-like escape driven by fractional Gaussian noise, *Phys. Rev. E* **81**, 041119 (2010).
- [67] A. P. Prudnikov, Y. Brychkov, and O. I. Marichev, *Integrals and Series*, vol. 3, More Special Functions (Gordon & Breach, New York, 1989).
- [68] S. A. Adelman, Fokker-Planck equations for simple non-Markovian systems, *J. Chem. Phys.* **64**, 124 (1976).
- [69] T. Guggenberger, A. V. Chechkin, and R. Metzler, Fractional Brownian motion in superharmonic potentials and non-Boltzmann stationary distributions, *J. Phys. A* **54**, 29LT01 (2021).
- [70] J. Friedrich, J. Peinke, A. Pumir, and R. Grauer, Explicit construction of joint multipoint statistics in complex systems, [arXiv:2105.03223](https://arxiv.org/abs/2105.03223).
- [71] A. G. Cherstvy, S. Thapa, Y. Mardoukhi, A. V. Chechkin, and R. Metzler, Time averages and their statistical variation for the Ornstein-Uhlenbeck process: Role of initial particle conditions and relaxation to stationarity, *Phys. Rev. E* **98**, 022134 (2018).